

Ring the initial Universe: the response of overdensity and transformed-density power spectra to initial spikes

Mark C. Neyrinck¹ and Lin Forrest Yang¹

¹*Department of Physics and Astronomy, The Johns Hopkins University, Baltimore, MD 21218, USA*

3 December 2024

ABSTRACT

We present an experiment in which we ‘ring’ a set of cosmological N -body-simulation initial conditions, placing spikes in its initial power spectrum at different wavenumber bins. We then measure where these spikes end up in the final conditions. In the usual, overdensity power spectrum, most sensitive to contracting and collapsing dense regions, initial power on slightly non-linear scales ($k \sim 0.3 h \text{ Mpc}^{-1}$) smears to smaller scales, coming to dominate the initial power once there. In log-density and Gaussianized-density power spectra, the sensitivity to low-density (expanding) as well as high-density regions produces a different response: initial spikes spread symmetrically in scale, both upward and downward. We also test the difference between a crude approximation of the Ly- α flux field, and its Gaussianized form. In the power spectrum of the reciprocal density, $1/(1 + \delta)$, spikes migrate to larger scales, indicating the magnifying effect voids have on small-scale modes. We give a toy model that qualitatively explains the symmetric power spreading in Gaussianized-density power spectra. Also, we discuss how to use this framework to estimate power-spectrum covariance matrices. This can be used to track the fate of information in the Universe, that takes the form of initial degrees of freedom, one random spike per initial mode.

Key words: large-scale structure of Universe – cosmology: theory

1 INTRODUCTION

Fluctuations in the present-epoch cosmic density field are rich in cosmological information. However, even for the theoretically straightforward real-space dark-matter field, the relation between the initial and final fluctuations is obscure on small scales. In the usual overdensity $\delta = \rho/\bar{\rho} - 1$, the shape of the power spectrum departs substantially from linear theory on small scales. A further obstacle to inferring initial information is the substantial covariance which arises in the δ power spectrum on small scales (Meiksin & White 1999). This covariance greatly reduces the Fisher information, i.e. increases error bars on cosmological parameters observable in principle (Rimes & Hamilton 2006; Neyrinck et al. 2006; Takahashi et al. 2009; Kiessling et al. 2011).

Fortunately, much of this apparently lost Fisher information can be recovered using a local 1-point probability density function (PDF) Gaussianizing transform, such as a logarithm or rank-order-Gaussianization (Neyrinck et al. 2009; Seo et al. 2011; Neyrinck 2011a; Yu et al. 2011). These Fisher analyses used measurements of final-conditions covariances in the power spectrum, which are related to the independent degrees of freedom resident there, but not directly to the initial degrees of freedom.

In this Letter, we explicitly track these initial degrees of freedom, in an N -body experiment in which we observe the results of ‘ringing’ the initial density field with initial power-spectrum spikes at different wavenumbers. This quantifies the ‘memory’ of initial

conditions (ICs) in the final field, but differently than the propagator (Crocco & Scoccimarro 2006, CS06), which can be thought of as a cross-correlation of a mode’s amplitude and phase in the initial and final conditions. Information in an initial mode gets deposited in larger or smaller-scale modes, but does not disappear, as a naive interpretation of a vanishing propagator might suggest.

We measure the response in the power spectra of a few transformed fields: $e^{-(1+\delta)}$; the log-density $\ln(1 + \delta)$; the rank-order-Gaussianized density $\text{Gauss}(\delta)$; and the reciprocal-density $\frac{1}{1+\delta}$. The ‘Gauss’ function is an increasing function, depending on the PDF of its argument, whose result has a Gaussian PDF. Explicitly, $\text{Gauss}(\delta) = \sqrt{2}\sigma \text{erf}^{-1}(2f_{<\delta} - 1 + 1/N)$, where $f_{<\delta}$ is the fraction of cells less-dense than δ , σ is the standard deviation of the Gaussian that δ ’s PDF is mapped onto, and N is the number of cells. Below, we set $\sigma = \sqrt{\text{Var}(\ln(1 + \delta))}$. So $\text{Gauss}(\delta)$ is essentially $\ln(1 + \delta)$ with its skewness removed.

These transformations increasingly emphasize low-density regions, where the initial fluctuations are the most pristine. We expect the different effective weightings provided by the transformations to affect the way power migrates in scale as structure forms. McCullagh et al. (2013) showed analytically using the Zel’dovich approximation (ZA, Zel’dovich 1970) that the baryon acoustic (BAO) peak location in the correlation function changes if a transform is applied to the field, based on the density regimes that the transform emphasizes. In δ , $\ln(1 + \delta)$, and $\frac{1}{1+\delta}$, the BAO peak location is slightly biased inward, nearly unbiased, and biased outward com-

arXiv:1305.1629v1 [astro-ph.CO] 7 May 2013

pared to linear theory. The present Letter carries these results to general power-spectrum features.

We investigate these particular transformations for various reasons. In a lognormal (Coles & Jones 1991), or nearly lognormal field, two-point statistics of the log-density capture a much greater fraction of the Fisher information in the field than those of δ (Neyrinck et al. 2009; Carron 2011; Carron & Neyrinck 2012). Forcing the one-point moments to zero, as Gaussianization does, generally decreases higher-order multi-point correlations as well, and allows two-point statistics to more effectively capture the information in a field. Also, the power spectrum of the log-density and Gaussianized density have an intriguingly nearly-linear shape, which this study addresses. $\frac{1}{1+\delta}$ is of some theoretical interest, being a simple quantity in a Lagrangian framework (just the Jacobian of the deformation tensor); also, it is rather insensitive to multi-streaming, which only further suppresses high-density regions. We investigate $e^{-(1+\delta)}$ because of its relevance to Ly- α -forest measurements; from a dark-matter simulation, it gives the flux, in the (poor) approximation that neutral hydrogen follows dark matter. It is of interest in the study of density transforms, since Gaussianization (Weinberg 1992) was tried in Ly- α -forest studies (Croft et al. 1998), but later works skipped that step (e.g. Croft et al. 2002). Without noise, $\text{Gauss}(\delta) = -\text{Gauss}(e^{-(1+\delta)})$, so comparing the results of these two transformations is a test of Gaussianization’s usefulness in Ly- α studies.

In Section 2, we describe the simulation suites and other techniques. In Section 3, we give our main results. In Section 4, we explain a crude toy model that qualitatively captures the migration of power in Gaussianized-density power spectra. In Section 5, we discuss estimating practical power-spectrum covariance matrices and Fisher information from these results.

2 METHODS

We ran three ensembles of 24 simulations: one ‘control’ simulation without initial power-spectrum spikes, and 23 simulations with spikes, each in a different power-spectrum bin. Previous numerical experiments have been run in which some Fourier modes are kept fixed, and others are changed (e.g. Little et al. 1991; Suhhonenko et al. 2011; Aragón-Calvo 2012). Our simulations, run using GADGET2 (Springel 2005), each have 256^3 particles in a $256 h^{-1}$ Mpc box, and ICs generated using the ZA at redshift $z = 127$. The simulations used vanilla Λ CDM cosmological parameters: $(h, \Omega_b, \Omega_{\text{cdm}}, \Omega_\Lambda, \sigma_8, n_s) = (0.73, 0.045, 0.205, 0.75, 0.8, 1)$. Each spike was inserted by multiplying the mode amplitudes in the corresponding bin by $\sqrt{2}$, holding all other aspects of the ICs fixed. As usual, each initial mode’s phase is random and, on average, uncorrelated to other phases. However, to avoid possible effects from spikes that arise randomly from cosmic variance, the amplitude of each initial mode at k is set to exactly $\sqrt{P(k)}$. So, the only difference between the three ensembles is in their sets of random phases. Because Fourier amplitudes are not drawn from a Rayleigh distribution as usual, some higher-order statistics within each box may be suppressed, but the simulations are suitable for their intended purpose, to track the migration of power.

On the scales investigated, $P_\delta \gg 1/n$, the P_δ shot noise. For the δ analysis, we use a cloud-in-cell (CIC) density assignment on a 256^3 grid. The largest wavenumber plotted is that where power spectra estimated with a nearest-grid-point (NGP) method departs noticeably from the CIC power spectra.

However, for $\ln(1+\delta)$, $\text{Gauss}(\delta)$, and especially $\frac{1}{1+\delta}$, care is

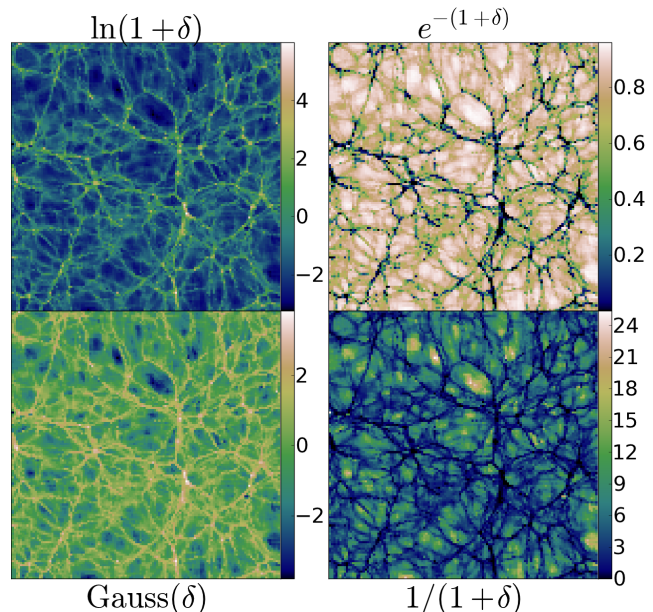


Figure 1. Plots of the transformed density-field slices from simulations used. The width of each panel is $128 h^{-1}$ Mpc, half the box size, and the pixel size is $1 h^{-1}$ Mpc. The Lagrangian-tessellation density estimate allows accurate density estimates deep within voids, with suppressed particle-discreteness effects compared to other methods.

required in density estimation because of sensitivity to low-density regions. The results also depend somewhat on the cell size to which the transforms are applied; here, we use $1 h^{-1}$ Mpc cells. We use what we call the Lagrangian Tessellation Field Estimator (LTFE, Abel et al. 2012; Shandarin et al. 2012), referencing the Delaunay and Voronoi Tessellation Field Estimators (DTFE, VTFE, e.g. Schaap & van de Weygaert 2000), which use Eulerian tessellations. Fig. 1 shows transformed-density slices measured this way, from our simulations. The Lagrangian tessellation has a more physical meaning than the Eulerian tessellations, although it has the drawback that it requires knowledge of the ICs, and thus cannot directly be applied to observations. In the LTFE, particles are treated not as mass blobs, but as vertices on a dark-matter sheet (see also Falck et al. 2012; Neyrinck 2012). For most purposes, this approximation is better than treating them as mass blobs, since a physical dark-matter particle is dozens of orders of magnitude lighter than a simulation ‘particle.’ Lagrangian space is tessellated into tetrahedra according to the initial cubic-lattice particle arrangement. Matter is uniformly deposited into tetrahedra, which often overlap in high-density regions where streams cross. No pixel is empty, since for each position, there is at least one tetrahedron that gets stretched across it. This method reveals fluctuations in low-density regions that would be difficult to see using a more naive density-estimation method. Much higher mass resolution would be necessary to measure $P_{1/(1+\delta)}$ using CIC.

Ideally, the LTFE would be computed in our cubic cells by computing the intersections of tetrahedra with each cubic cell. However, for speed, we instead sample the density on a cubic lattice of points. For each tetrahedron enclosing a given lattice point, we add densities inversely proportional to the tetrahedron. To reduce the noise from this point-sampling, each grid point comes from an eightfold density super-sampling; the density is measured on a 512^3 grid, which we then average down to a 256^3 grid. Even so,

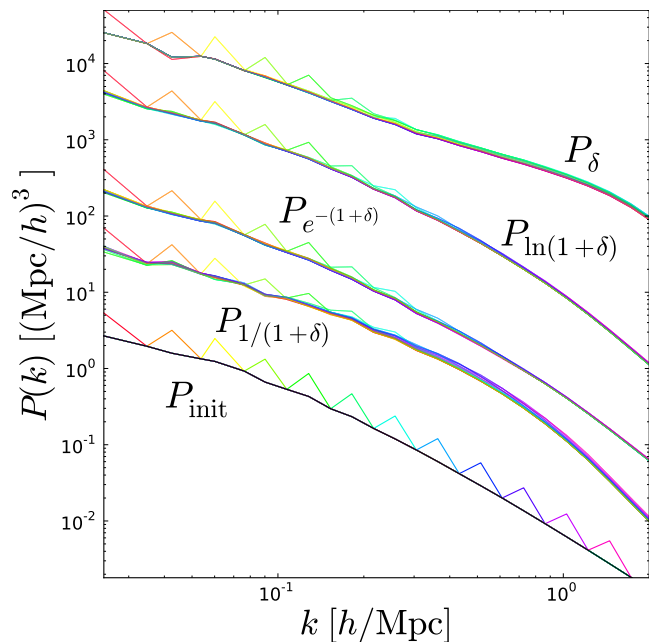


Figure 2. From top to bottom, $z = 0$ power spectra from initial-spike simulations of various transformed-density power spectra, along with the spiked initial conditions at $z = 127$. Power spectra are rainbow-colored according to the wavelength of their initial spike, from short (violet) to long (red). $P_{1/(1+\delta)}$ is divided by 10^3 for clarity. $P_{\text{Gauss}(\delta)}$, investigated below, is omitted because it is almost indistinguishable from $P_{\ln(1+\delta)}$.

the process requires much more computation than e.g. CIC, so we implemented a fast GPU code employing CUDA technology.

3 RESULTS

Fig. 2 shows various power spectra at $z = 0$ from one ensemble of spiked simulations. Also shown is the initial density field used to generate the ICs, P_{init} . At large scales, initial spikes are preserved in each power spectrum. But on small scales, each power spectrum behaves differently. At $k \sim 1 h \text{ Mpc}^{-1}$, the initial scales dominating P_δ correspond to the green color (larger scales), while the initial scales dominating $P_{1/(1+\delta)}$ correspond to violet (smaller scales).

Figs. 3 and 4 show the results more clearly, using the linear-response matrix

$$G_{ij} \equiv \frac{\partial \ln P(k_i)}{\partial \ln P^{\text{init}}(k_j)}. \quad (1)$$

We use three ensembles of simulations to lower the realization-to-realization variance in the measured G_{ij} , which is typically at the $\sim 10\%$ level, depending on scale. Fixing all mode amplitudes to their ensemble-mean values reduces this variance, but differences in random phases still produce fluctuations. The reported value of each G_{ij} matrix element is the median among the three ensembles.

In δ , the migration of power is qualitatively as in Hamilton et al. (1991) and Peacock & Dodds (1996): power moves from large to small scales. However, a fixed initial scale does not migrate to a fixed non-linear scale. Translinear ($k \sim 0.3 h \text{ Mpc}^{-1}$) initial scales end up smeared over a wide range of smaller scales. The result is that small ($k \sim 1 h \text{ Mpc}^{-1}$) final scales are dominated by translinear initial modes, and are insensitive to initial power at their own comoving wavenumber. Indeed, initial power inserted at

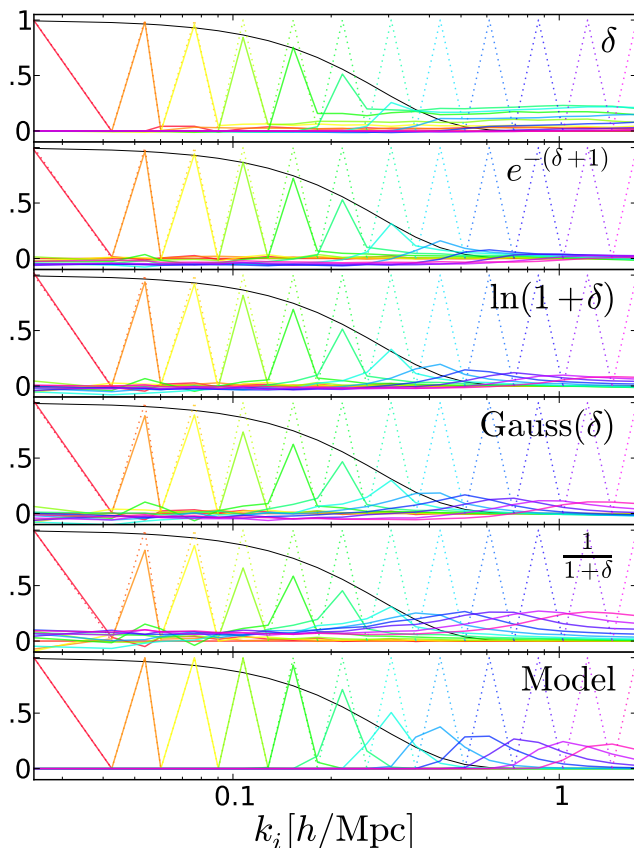


Figure 3. Plots of the matrix G_{ij} , defined in Eq. (1), showing the response of final-conditions power spectra to initial spikes. The spikes in the initial conditions are shown with dotted curves, rainbow-colored from red to violet going from low to high frequency. Corresponding power spectra of final-conditions simulations appear as solid curves. From top to bottom, the final-conditions resting place of a moderate-scale (e.g. green) spike moves from small to large scales, as each transformation increasingly emphasizes underdense regions. For clarity, power spectra from only odd-numbered spikes are shown. The ‘model’ is a toy model of power spreading based on a local spherical collapse or expansion of volume elements, given in Eq. (4). The black curves show the density propagator (CS06).

$k \sim 1 h \text{ Mpc}^{-1}$ hardly affects P_δ over the scales measured, although it might show up at smaller scales in higher-resolution simulations. Black curves show an approximation of the $z = 0$ density propagator, a Gaussian with $\sigma_k = 0.2 h \text{ Mpc}^{-1}$ (CS06). The propagator is a cross-correlation of modes in the initial and final conditions, sensitive to both amplitudes and phases, and, as expected, it follows G_{ij}^δ 's diagonal quite well.

In $\ln(1 + \delta)$ and $\text{Gauss}(\delta)$, the behavior is different. Power spreads out, moving not just from large to small scales, but vice-versa, rather symmetrically. This makes sense: P_δ is mostly sensitive to high-density regions, where fluctuations have contracted. $P_{\ln(1+\delta)}$ and $P_{\text{Gauss}(\delta)}$, on the other hand, are sensitive to dense regions, but also to low-density regions, where fluctuations have expanded. In fact, initial peaks migrate to a bit larger scales than they were initially (visible as slight upturns in Fig. 4). There are a couple of possible reasons for this upturn: underdense regions, even if equal by mass, dominate by volume. Also, in overdense regions, many fluctuations completely collapse, perhaps leaving no clear signal in the power spectrum. In underdense final regions, however, almost all fluctuations remain, stretched-out compared to the

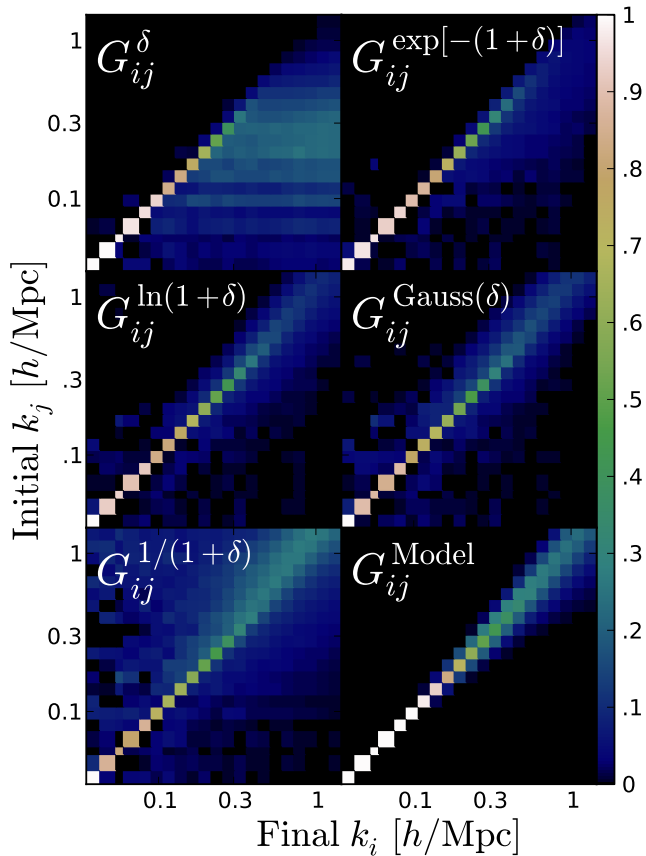


Figure 4. G_{ij} 's as in Fig. 3, shown in matrix form.

ICs. Indeed, in the $\frac{1}{1+\delta}$ field, in which underdense regions receive almost all weight, the high value of $G_{ij}^{1/(1+\delta)}$ above the diagonal indicates this comoving expansion of fluctuations. This explicitly confirms the magnifying effect (Aragon-Calvo & Szalay 2013) that voids have on initially small scales.

Going from δ down to $\frac{1}{1+\delta}$ in Fig. 3, the sensitivity to small-scale initial power increases substantially. There is a trade-off on large scales, though: diagonal entries decrease slightly, and off-diagonal terms fluctuate increasingly from zero. Large-scale modes, exceeding the scales of typical displacements, are fixed in P_δ by mass conservation, but after a transformation, this is no longer assured, so some fluctuations in large-scale mode amplitudes occur. However, there seems to be no systematic trend in these fluctuations; averaging over many realizations of phases, it seems that these off-diagonal elements would average to zero.

4 TOY MODEL FOR POWER SPREADING

A toy model of $G_{ij}^{\text{Gauss}(\delta)}$ based on Lagrangian dynamics captures its behavior qualitatively. The model, which does not explicitly consider the Gaussianization process, is that initial fluctuations expand or contract according to the local density, and that the final $P_{\text{Gauss}(\delta)}$ manages to pick up every fluctuation at the scales where it has expanded or contracted in final conditions. In reality, some initial fluctuations collapse, or otherwise escape detection by $P_{\text{Gauss}(\delta)}$, but the approximation here is that they do not.

Consider fluctuations imprinted on initial pixels of equal Lagrangian size that expand or contract according to the local den-

sity. In the ZA, $\nabla_q \cdot \Psi = -\delta_{\text{lin}}$, where $\Psi = \mathbf{x} - \mathbf{q}$ is the Lagrangian displacement field, and δ_{lin} is the linearly extrapolated initial density. Approximating each pixel's expansion or contraction as isotropic, with Lagrangian displacement-divergence 'stretching' parameter $\psi \equiv \nabla_q \cdot \Psi$, each of its 3 dimensions will scale by a factor $1 + \psi/3$. On logarithmic plots such as Figs. 3 and 4, a fluctuation occupying pixels that stretch in such a way gets shifted by $s \equiv -\ln(1 + \psi/3)$, the minus sign because of the reciprocal from working in Fourier space.

A Gaussian PDF of ψ , with variance σ , can be transformed into a mass-weighted (Lagrangian volume) PDF of s in the ZA:

$$\mathcal{P}(s) = \mathcal{P}(\psi) \left| \frac{d\psi}{ds} \right| = \frac{3 \exp[-(3e^{-s} - 1)^2 / (2\sigma^2) - s]}{\sqrt{2\pi\sigma^2}}, \quad (2)$$

where \mathcal{P} denotes a probability distribution.

Alternatively, a spherical-collapse approximation can be used for the behavior of ψ , where ψ_z is its ZA value (Mohayaee et al. 2006; Neyrinck 2013),

$$\psi_{\text{sc}} = 3 \left[\left(1 + \frac{2}{3} \psi_z \right)^{1/2} - 1 \right]. \quad (3)$$

This uses an approximation for the evolution of a volume element found by Bernardeau (1994), valid in the limit of low matter density. It gives the following distribution of s :

$$\mathcal{P}(s) ds = \frac{(3/2) \exp[-(3/2)(e^{-2s} - 1)^2 / (2\sigma^2) - 2s]}{\sqrt{2\pi\sigma^2}} \quad (4)$$

Both Eqs. (2) and (4) can be approximated by a Gaussian of dispersion $\sigma/3$ for small σ .

The final panels of Figs. 3 and 4 show G_{ij} in this model. The assumption is that Eq. (4) gives the shapes of the curves into which spikes broaden in Fig. 3. Each j row is normalized so that all initial fluctuations contribute to some final wavenumber, i.e. so that for all j , $\sum_i G_{ij}^{\text{Model}} = 1$. Physically, this would describe G_{ij} for a density variable that manages to capture all Lagrangian volumes, both expanding and contracting. It is not surprising that G_{ij}^{Model} has higher amplitude on small scales than any measured G_{ij} , since some fluctuations doubtless evade notice by any final power spectrum, i.e. $\sum_i G_{ij} < 1$ generally. We estimate σ^2 in Eq. (4) as the variance in top-hat spheres of radius $2\pi/k_j$ in linear theory. This model is quite naive; for instance, it assumes an equal-Lagrangian-volume (i.e. mass) weighting, rather than a more appropriate (Eulerian) volume-weighting. Still, the model captures the qualitative behavior of $G_{ij}^{\text{Gauss}(\delta)}$, although it may underestimate the variance at low k_j , and overestimates $G_{ij}^{\text{Gauss}(\delta)}$ along the diagonal.

5 COVARIANCE MATRICES AND INFORMATION

G_{ij} can be used to estimate power-spectrum covariances, as well. Usually, covariance matrices are measured directly from ensembles of final density fields, and it is interesting to compare this approach with the result of directly tracking initial-conditions degrees of freedom. A linear model of a fluctuation away from the mean in the final-conditions $\ln P_i$ (investigated instead of P_i for algebraic simplicity) is, summing over repeated indices,

$$\Delta \ln P_i = \frac{\partial \ln P_i}{\partial \ln P_j^{\text{init}}} \Delta \ln P_j^{\text{init}} = G_{ij} \Delta \ln P_j^{\text{init}}, \quad (5)$$

giving

$$C_{ij} = \langle \Delta \ln P_i \Delta \ln P_j \rangle = \langle G_{ik} \Delta \ln P_k^{\text{init}} G_{jl} \Delta \ln P_l^{\text{init}} \rangle. \quad (6)$$

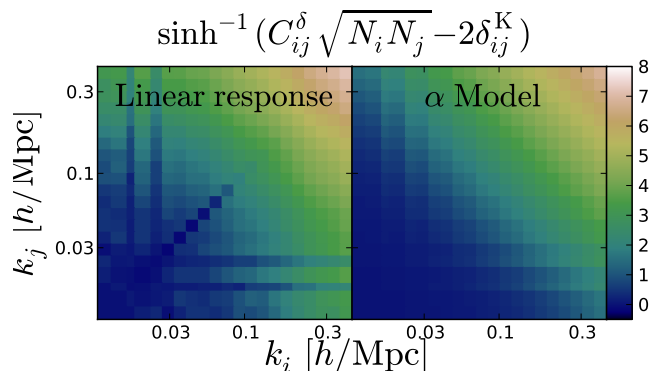


Figure 5. The non-Gaussian part of the δ power-spectrum covariance T_{ij} , as measured from G_{ij}^δ using the linear-response model of Eq. (6), and using an ‘ α model’ approximation to T_{ij} found in (Neyrinck 2011b). Because of the steep increase, we use a \sinh^{-1} transform for plotting, which becomes logarithmic for large values of its argument. While the α model should not be taken too seriously as it is only an approximation, the qualitative agreement (except, perhaps, far from the diagonal) between the two plots suggests that the linear-response model captures most of the relevant effects.

Since the Gaussian $C_{ij}^{\text{init}} \equiv \langle \Delta \ln P_i^{\text{init}} \Delta \ln P_j^{\text{init}} \rangle = 2\delta_{ij}^K/N_i$, where N_i is the number of modes in bin i ,

$$C = \mathbf{G}C^{\text{init}}\mathbf{G}^\top. \quad (7)$$

Now, suppose we want to estimate all $\ln P_i^{\text{init}}$ from the final power spectrum. The Fisher matrix F_{ij} to use to predict constraints on this initial power in bins i and j would be

$$F_{ij} = \frac{\partial \ln P_k}{\partial \ln P_i^{\text{init}}} (\mathbf{C}^{-1})_{kl} \frac{\partial \ln P_l}{\partial \ln P_j^{\text{init}}} = G_{ki} (\mathbf{C}^{-1})_{kl} G_{lj}, \quad (8)$$

or

$$F = \mathbf{G}^\top (\mathbf{G}C^{\text{init}}\mathbf{G}^\top)^{-1} \mathbf{G} = (\mathbf{C}^{\text{init}})^{-1}. \quad (9)$$

So the covariance matrix of parameters that consist of the initial power spectrum in bins is just the initial, Gaussian power-spectrum covariance matrix. This suggests no Fisher-information loss!

However, this calculation assumes that the final power spectrum is an entirely deterministic, invertible, linear transformation of the initial power spectrum, with no sources of noise. This is not the case; it neglects at least a couple of things: the non-linear coupling of pairs of power-spectrum spikes, and realization-to-realization fluctuations in the G_{ij} matrix, which can depend on both the power spectrum itself, and also on mode correlations (present even in a Gaussian field) that affect the halo mass function, which substantially affects translinear-scale power, at least in the halo model (Neyrinck et al. 2006).

One neglected factor that can be investigated in a straightforward extension of the present framework is the non-linear coupling of spike pairs. But this would involve a simulation for each pair of wavenumber bins, i.e. with 23 bins, $23 \times 22 = 506$ additional simulations. We plan to run this brute-force ensemble in future work. For now, we compare the covariance matrix from Eq. (5) to one estimated otherwise.

Fig. 5 shows the non-Gaussian part of the δ power-spectrum covariance $T_{ij}^\delta \equiv C_{ij}^\delta (N_i N_j)^{1/2} - \delta_{ij}^K$, both in the linear-response model from G_{ij}^δ in Eq. (6), and from the fluctuating-multiplicative-bias model of Neyrinck (2011b), a rather accurate approximation to the covariance as measured from the Coyote Universe simulations (Lawrence et al. 2010). In this model, the non-Gaussian

covariance is given by $T_{ij}^\delta = \alpha(N_i N_j)^{1/2}$, where α is the fractional realization-to-realization variance of the nonlinear density-field variance in nonlinear-scale cells. We use $\alpha = 0.0035$ for this plot, which is α at $z = 0$ as found by Neyrinck (2011b), scaled to the $(256h^{-1} \text{ Mpc})^3$ volume of the present simulations.

We emphasize that the α model is approximate, but qualitatively, it agrees with the linear-response model rather well, suggesting that additional terms in the covariance may indeed be subdominant. The main discrepancies are in highly off-diagonal terms.

6 CONCLUSIONS

We used an N -body experiment to track where initial power-spectrum features get deposited in final-conditions density power spectra. For the usual overdensity field δ , our results qualitatively agree with the common wisdom that initial power migrates from large to small scales. However, this seems to be largely because the δ field is dominated by overdense spikes. When the density is transformed to have a more-Gaussian PDF, increasing the statistical weight of low-density regions (where patches imprinted with initial fluctuations expand rather than contract in comoving coordinates), initial spikes spread rather symmetrically, both upward and downward in scale. In fact, in $P_{1/(1+\delta)}$, almost exclusively sensitive to underdense regions, initially small scales are magnified, as pointed out by Aragon-Calvo & Szalay (2013).

The spread of power in the Gaussianized variables such as $\ln(1+\delta)$ is qualitatively captured by a toy model we give, in which patches imprinted with initial fluctuations expand or contract according to a spherical-collapse model. In the future, it would be interesting to refine this model for greater accuracy, and investigate whether it might be modified successfully to other power spectra.

We also begin to apply our results to the theoretical question of how degrees of freedom present in the initial density field, essentially a sum of many spikes such as the ones we use, disappear from the final-conditions, coarse-grained density field. However, this will require further measurements, because in our framework, fluctuations in the final power spectrum are a linear, invertible transformation of the initial power spectrum, given by a matrix G_{ij} . In reality, though, information is lost because of a few neglected effects, which we will analyze in future work. We do, however, find that G_{ij} gives a rather accurate description of the P_δ covariance matrix, suggesting that one of these effects (the nonlinear coupling of spike pairs) is not dominant. Thus, ‘ringing’ the initial power spectrum as we do offers an interesting technique to estimate power-spectrum covariances and Fisher information, by tracking the true, initial degrees of freedom in the Universe.

ACKNOWLEDGMENTS

We thank Nuala McCullagh, Julien Carron, Miguel Aragón-Calvo, Xin Wang, István Szapudi and Alex Szalay for stimulating discussions. We are grateful for support from NSF OIA grant CDI-1124403, and the Gordon and Betty Moore Foundation, and MCN is grateful for support from a New Frontiers in Astronomy and Cosmology grant from the Sir John Templeton Foundation.

REFERENCES

- Abel, T., Hahn, O., & Kaehler, R. 2012, MNRAS, 427, 61, 1111.3944

- Aragón-Calvo, M. A. 2012, MNRAS, submitted, 1210.7871
Aragon-Calvo, M. A., & Szalay, A. S. 2013, MNRAS, 428, 3409, 1203.0248
Bernardeau, F. 1994, ApJ, 427, 51, arXiv:astro-ph/9311066
Carron, J. 2011, ApJ, 738, 86, 1105.4467
Carron, J., & Neyrinck, M. C. 2012, ApJ, 750, 28, 1201.1444
Coles, P., & Jones, B. 1991, MNRAS, 248, 1
Croce, M., & Scoccimarro, R. 2006, Phys. Rev. D, 73, 063520, arXiv:astro-ph/0509419
Croft, R. A. C., Weinberg, D. H., Bolte, M., Burles, S., Hernquist, L., Katz, N., Kirkman, D., & Tytler, D. 2002, ApJ, 581, 20, arXiv:astro-ph/0012324
Croft, R. A. C., Weinberg, D. H., Katz, N., & Hernquist, L. 1998, ApJ, 495, 44, arXiv:astro-ph/9708018
Falck, B. L., Neyrinck, M. C., & Szalay, A. S. 2012, ApJ, 754, 126, 1201.2353
Hamilton, A. J. S., Kumar, P., Lu, E., & Matthews, A. 1991, ApJL, 374, L1
Kiessling, A., Taylor, A. N., & Heavens, A. F. 2011, MNRAS, 416, 1045, 1103.3245
Lawrence, E., Heitmann, K., White, M., Higdon, D., Wagner, C., Habib, S., & Williams, B. 2010, ApJ, 713, 1322, 0912.4490
Little, B., Weinberg, D. H., & Park, C. 1991, MNRAS, 253, 295
McCullagh, N., Neyrinck, M. C., Szapudi, I., & Szalay, A. S. 2013, ApJL, 763, L14, 1211.3130
Meiksin, A., & White, M. 1999, MNRAS, 308, 1179, arXiv:astro-ph/9812129
Mohayaee, R., Mathis, H., Colombi, S., & Silk, J. 2006, MNRAS, 365, 939, arXiv:astro-ph/0501217
Neyrinck, M. C. 2011a, ApJ, 742, 91, 1105.2955
———. 2011b, ApJ, 736, 8, 1103.5476
———. 2012, MNRAS, 427, 494, 1202.3364
———. 2013, MNRAS, 428, 141, 1204.1326
Neyrinck, M. C., Szapudi, I., & Rimes, C. D. 2006, MNRAS, 370, L66, arXiv:astro-ph/0604282
Neyrinck, M. C., Szapudi, I., & Szalay, A. S. 2009, ApJL, 698, L90, 0903.4693
Peacock, J. A., & Dodds, S. J. 1996, MNRAS, 280, L19, arXiv:astro-ph/9603031
Rimes, C. D., & Hamilton, A. J. S. 2006, MNRAS, 371, 1205, arXiv:astro-ph/0511418
Schaap, W. E., & van de Weygaert, R. 2000, A&A, 363, L29, arXiv:astro-ph/0011007
Seo, H.-J., Sato, M., Dodelson, S., Jain, B., & Takada, M. 2011, ApJL, 729, L11, 1008.0349
Shandarin, S., Habib, S., & Heitmann, K. 2012, Phys. Rev. D, 85, 083005, 1111.2366
Springel, V. 2005, MNRAS, 364, 1105, arXiv:astro-ph/0505010
Suhhonenko, I. et al. 2011, A&A, 531, A149, 1101.0123
Takahashi, R. et al. 2009, ApJ, 700, 479, 0902.0371
Weinberg, D. H. 1992, MNRAS, 254, 315
Yu, Y., Zhang, P., Lin, W., Cui, W., & Fry, J. N. 2011, Phys. Rev. D, 84, 023523, 1103.2858
Zel'dovich, Y. B. 1970, A&A, 5, 84